Flight Dynamic Response of Spinning Projectiles to Lateral Impulsive Loads

G. R. Cooper
Research Physicist
Weapons and Materials Research Directorate,
U.S. Army Research Laboratory,
Aberdeen Proving Ground, MD

Mark Costello
Associate Professor, Member ASME
Department of Mechanical Engineering,
Oregon State University,
Corvallis, OR 97331

The linear theory for spinning projectiles is extended to account for the application of a simple lateral square impulse activated during free flight. Analytical results are shown to produce simple contributions to the familiar aerodynamic jump formulation. Inquiries regarding jump smearing caused by nonzero impulse length are addressed and answered. The formulation shows for sufficiently long-term target interception, lateral impulse trajectory response for a guided projectile is independent of when the impulse is activated during the yaw cycle. Simple limits show the presented results reducing to those previously found for a zero-spin projectile acted upon by a singular lateral impulse.
[DOI: 10.1115/1.1789976]

Introduction

The continuing development of microelectromechanical systems (MEMS) is pointing to the possibility of mounting complete sensor systems on medium- and small-caliber projectiles as part of an actively controlled smart munition. Two important technical challenges in achieving this goal are the development of small, rugged sensor suites and control mechanisms. With regard to the development of control mechanisms, several concepts have emerged that produce controllable impulsive lateral forces on a projectile body. For example, Harkins and Brown [1] considered the use of a set of lateral pulse jets or squibs to reduce dispersion of a rocket by firing squibs to minimize projectile pitch and yaw rate. For the notional cases evaluated, dispersion was reduced by a factor of 5. Jitpraphai and Costello [2] considered the same type of control mechanism and used a trajectory tracking flight control system to improve impact point performance of a direct fire rocket equipped with a ring of squibs. Amitay et al. [3] considered the use of synthetic jet actuators as a control mechanism on lifting bodies. For a spinning projectile incorporating a synthetic jet actuator for control, the synthetic jet actuator is activated over a small portion of a roll cycle leading to a train of lateral pulse forces acting on the projectile near the synthetic jet actuator cavity.

The design of flight control systems for fin stabilized configurations is well established in the missile community and the control response to force and moment inputs is reasonably well understood. Generally these configurations are treated largely in the same manner as airplanes. While the uncontrolled dynamics of spinning projectiles (both fin stabilized and spin stabilized) has been extensively studied in the ballistics community, issues with regard to control response have received considerably less attention due to the lack of practical application of control technology to spinning projectiles. Using projectile linear theory, this paper analytically investigates several aspects of the response of a spinning projectile to lateral pulse forces including swerve response magnitude and phase angle, impulse force smearing, and yaw cycle pulse timing. The paper begins with a discussion of the basic projectile dynamic model followed by judicious simplifications to these equations that result in the projectile linear theory equations. The solution of the projectile linear theory equations is used to shed light on intuitive and subtle factors that influence swerve response of a projectile exposed to lateral impulsive loads.

Contributed by the Dynamic Systems, Measurement, and Control Division of THE AMERICAN SOCIETY OF MECHANICAL ENGINEERS for publication in the ASME JOURNAL OF DYNAMIC SYSTEMS, MEASUREMENT, AND CONTROL. Manuscript received by the ASME Dynamic Systems and Control Division March 6, 2003; final revision, August 21, 2003. Associate Editor: R. Mukherjee.

Projectile Dynamic Model

It is well known that the motion of most projectile configurations can be captured using a rigid body 6 degrees of freedom dynamic model [4,5]. The degrees of freedom include three position components of the mass center of the projectile as well as three Euler orientation angles of the body. Figures 1 and 2 show schematics of the dynamic model degrees of freedom. The equations of motion are provided in Eqs. (1–4).

$$\begin{Bmatrix}\dot{x}\\ \dot{y}\\ \dot{z}\end{Bmatrix}=\begin{bmatrix} c_\theta c_\psi & s_\phi s_\theta c_\psi - c_\phi s_\psi & c_\phi s_\theta c_\psi + s_\phi s_\psi \\ c_\theta s_\psi & s_\phi s_\theta s_\psi + c_\phi c_\psi & c_\phi s_\theta s_\psi - s_\phi c_\psi \\ -s_\theta & s_\phi c_\theta & c_\phi c_\theta \end{bmatrix}\begin{Bmatrix}u\\ v\\ w\end{Bmatrix}; \quad (1)$$

$$\begin{Bmatrix}\dot{\phi}\\ \dot{\theta}\\ \dot{\psi}\end{Bmatrix}=\begin{bmatrix}1 & s_\phi t_\theta & c_\phi t_\theta \\ 0 & c_\phi & -s_\phi \\ 0 & s_\phi/c_\theta & c_\phi/c_\theta\end{bmatrix}\begin{Bmatrix}p\\ q\\ r\end{Bmatrix}=\begin{bmatrix}1 & 0 & t_\theta \\ 0 & 1 & 0 \\ 0 & 0 & 1/c_\theta\end{bmatrix}\begin{Bmatrix}p\\ \tilde{q}\\ \tilde{r}\end{Bmatrix}; \quad (2)$$

$$\begin{Bmatrix}\dot{u}\\ \dot{v}\\ \dot{w}\end{Bmatrix}=\begin{Bmatrix}X/m\\ Y/m\\ Z/m\end{Bmatrix}-\begin{bmatrix}0 & -r & q\\ r & 0 & -p\\ -q & p & 0\end{bmatrix}\begin{Bmatrix}u\\ v\\ w\end{Bmatrix}; \quad (3)$$

$$\begin{Bmatrix}\dot{p}\\ \dot{q}\\ \dot{r}\end{Bmatrix}=I^{-1}\left[\begin{Bmatrix}L\\ M\\ N\end{Bmatrix}-\begin{bmatrix}0 & -r & q\\ r & 0 & -p\\ -q & p & 0\end{bmatrix}I\begin{Bmatrix}p\\ q\\ r\end{Bmatrix}\right]. \quad (4)$$

The applied forces in the body frame that appear in Eq. (5) contain contributions from weight (W), air loads (A), and lateral pulse forces (C),

$$\begin{Bmatrix}X\\ Y\\ Z\end{Bmatrix}=\begin{Bmatrix}X_W\\ Y_W\\ Z_W\end{Bmatrix}+\begin{Bmatrix}X_A\\ Y_A\\ Z_A\end{Bmatrix}+\begin{Bmatrix}X_C\\ Y_C\\ Z_C\end{Bmatrix}. \quad (5)$$

The weight force resolved into projectile body coordinates is given by Eq. (6),

$$\begin{Bmatrix}X_W\\ Y_W\\ Z_W\end{Bmatrix}=mg\begin{Bmatrix}-s_\theta\\ s_\phi c_\theta\\ c_\phi c_\theta\end{Bmatrix}. \quad (6)$$

The air loads are split in two components, the standard aerodynamic forces and the Magnus forces.

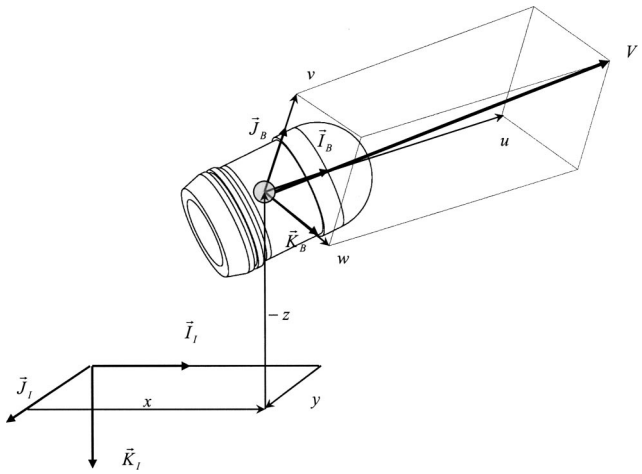

Fig. 1 Example of a nonuniform strain field

$$\begin{Bmatrix} X_A \\ Y_A \\ Z_A \end{Bmatrix} = \begin{Bmatrix} X_{AS} \\ Y_{AS} \\ Z_{AS} \end{Bmatrix} + \begin{Bmatrix} X_{AM} \\ Y_{AM} \\ Z_{AM} \end{Bmatrix}. \tag{7}$$

Equation (8) gives the standard air loads acting at the aerodynamic center of pressure,

$$\begin{Bmatrix} X_{AS} \\ Y_{AS} \\ Z_{AS} \end{Bmatrix} = -q_a \begin{Bmatrix} C_{X0} + C_{X2}\dfrac{(v^2+w^2)}{V^2} \\ C_{Y0} + C_{NA}v/V \\ C_{Z0} + C_{NA}w/V \end{Bmatrix}; \tag{8}$$

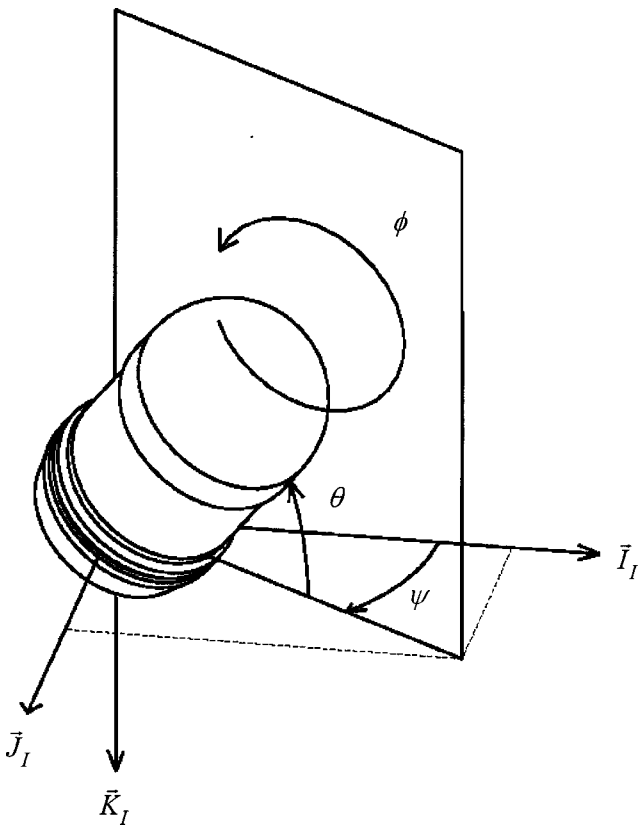

Fig. 2 GA flowchart

where

$$q_a = \tfrac{1}{8}\rho(u^2+v^2+w^2)\pi D^2; \tag{9}$$

$$V = \sqrt{u^2+v^2+w^2}. \tag{10}$$

The Magnus aerodynamic force acts at the Magnus center of pressure,

$$\begin{Bmatrix} X_{AM} \\ Y_{AM} \\ Z_{AM} \end{Bmatrix} = -q_a \begin{Bmatrix} 0 \\ \dfrac{pDC_{NPA}w}{2V} \\ \dfrac{-pDC_{NPA}v}{2V} \end{Bmatrix}. \tag{11}$$

The lateral pulse force is modeled as an impulse that acts on an arbitrary point on the body,

$$\begin{Bmatrix} X_C \\ X_C \\ Z_C \end{Bmatrix} = \begin{Bmatrix} 0 \\ Y_I \\ Z_I \end{Bmatrix} d(t). \tag{12}$$

In Eq. (12), Y_I and Z_I represent the lateral components of the impulse. The total magnitude of the impulse on the projectile is $F_I = \sqrt{Y_I^2 + Z_I^2}$. The function $d(t)$ is a constant positive value when the pulse is active and is zero otherwise. This function integrates to unity for a single pulse.

The applied moments about the projectile mass center are due to aerodynamic forces and moments (A) as well as pulse forces (C),

$$\begin{Bmatrix} L \\ M \\ N \end{Bmatrix} = \begin{Bmatrix} L_{SA} \\ M_{SA} \\ N_{SA} \end{Bmatrix} + \begin{Bmatrix} L_{UA} \\ M_{UA} \\ N_{UA} \end{Bmatrix} + \begin{Bmatrix} L_C \\ M_C \\ N_m \end{Bmatrix}. \tag{13}$$

The aerodynamic moments caused by standard and Magnus air loads are computed with a cross product between the distance vector from the mass center to the force application point and the force itself. An unsteady aerodynamic damping moment is also present, which provides a damping source for angular motion,

$$\begin{Bmatrix} L_{UA} \\ M_{UA} \\ N_{UA} \end{Bmatrix} = q_a D \begin{Bmatrix} C_{DD} + \dfrac{pDC_{LP}}{2V} \\ \dfrac{qDC_{MQ}}{2V} \\ \dfrac{rDC_{MQ}}{2V} \end{Bmatrix}. \tag{14}$$

All aerodynamic coefficients and the center of pressures are a function of the Mach number of the projectile mass center. The dynamic model previously described is highly nonlinear due to both three-dimensional rotational kinematics expressions and the presence of complex aerodynamic forces. The applicability of the equations of motion shown prior, have been validated over the past 60 years at aeroballistic ranges throughout the world [5].

Projectile Linear Theory

Pressed with the need to predict the trajectory and stability of a ballistic shell so that useful performance data could be generated with primitive computers, early ballisticians vigorously investigated mathematical simplifications to the equations of motion of a

projectile. What emerged over time was a set of simplified and solvable, yet accurate linear differential equations which today is commonly termed ''projectile linear theory.''

The governing equations previously developed are expressed in the body reference frame. In projectile linear theory, the lateral translational and rotational velocity components are transformed to a nonrolling reference frame. The nonrolling frame or so-called fixed plane frame proceeds with only precession and nutation rotations from an inertial reference frame. Components of linear and angular body velocities in the fixed plane frame can be computed from the body frame components of the same vector through a single axis rotational transformation. For example, the body frame components of the projectile mass center velocity are transformed to the fixed plane frame by

$$\begin{Bmatrix} \tilde{u} \\ \tilde{v} \\ \tilde{w} \end{Bmatrix} = \begin{Bmatrix} 1 & 0 & 0 \\ 0 & \cos\phi & \sin\phi \\ 0 & -\sin\phi & \cos\phi \end{Bmatrix} \begin{Bmatrix} u \\ v \\ w \end{Bmatrix}. \tag{15}$$

It should be noted that the $\tilde{\vdots}$ superscript indicates the vector components are described in the fixed plane reference frame. In projectile linear theory, a change of variables from station line velocity component, u, to total velocity, V, is performed. Equations (16) and (17) relate V and u and their derivatives.

$$V = \sqrt{u^2+v^2+w^2} = \sqrt{u^2+\tilde{v}^2+\tilde{w}^2}; \tag{16}$$

$$\frac{dV}{dt} = \frac{u\dfrac{du}{dt}+v\dfrac{dv}{dt}+w\dfrac{dw}{dt}}{V} = \frac{u\dfrac{du}{dt}+\tilde{v}\dfrac{d\tilde{v}}{dt}+\tilde{w}\dfrac{d\tilde{w}}{dt}}{V}; \tag{17}$$

A change of variables from time, t, to dimensionless arc length, s, is also made. Equation (18), as defined by Murphy [4], gives the dimensionless arc length.

$$s = \frac{1}{D}\int_0^t V dt. \tag{18}$$

Equations (19) and (20) relate time and arc length derivatives of a given quantity ζ. Dotted terms refer to time derivatives, and primed terms denote dimensionless arc length derivatives,

$$\dot{\zeta} = \left(\frac{D}{V}\right)\zeta'; \tag{19}$$

$$\ddot{\zeta} = \left(\frac{D}{V}\right)^2\left[\zeta'' + \frac{V'}{V}\zeta'\right]. \tag{20}$$

In projectile linear theory, several assumptions regarding the relative size of different quantities are made to simplify the analysis. Euler yaw and pitch angles are small so that $\sin(\theta)\approx\theta$, $\cos(\theta)\approx 1$, $\sin(\psi)\approx\psi$, and $\cos(\psi)\approx 1$ and the aerodynamic angle of attack is small so that $\alpha=\tilde{w}/V$ and $\beta=\tilde{v}/V$. The projectile is mass balanced such that $I_{XY}=I_{XZ}=I_{YZ}=0$ and $I_{ZZ}=I_{YY}\Rightarrow I_{YY}=I_{ZZ}\equiv I_Y$. The projectile is aerodynamically symmetric such that $C_{Y0}=C_{Z0}=0$. Quantities V and ϕ are large compared to θ, ψ, q, r, v, and w, such that products of small quantities and their derivatives are negligible. Application of these assumptions results in Eqs. (21–30).

$$x' = D; \tag{21}$$

$$y' = \frac{D}{V}\tilde{v} + D\psi; \tag{22}$$

$$z' = \frac{D}{V}\tilde{w} - D\theta; \tag{23}$$

$$\phi' = \frac{D}{V}p; \tag{24}$$

$$\theta' = \frac{D}{V}\tilde{q}; \tag{25}$$

$$\psi' = \frac{D}{V}\tilde{r}; \tag{26}$$

$$V' = -\frac{\rho S D C_{XO}}{2m}V - \frac{Dg\theta}{V}; \tag{27}$$

$$p' = \frac{\rho S D^2 C_{LDD}}{2I_X}V + \frac{\rho S D^3 C_{LP}}{4I_X}p; \tag{28}$$

$$\begin{Bmatrix} \tilde{v}' \\ \tilde{w}' \\ \tilde{q}' \\ \tilde{r}' \end{Bmatrix} = \begin{bmatrix} -A & 0 & 0 & -D \\ 0 & -A & D & 0 \\ B/D & C/D & E & -F \\ -C/D & B/D & F & E \end{bmatrix} \begin{Bmatrix} \tilde{v} \\ \tilde{w} \\ \tilde{q} \\ \tilde{r} \end{Bmatrix} + \begin{Bmatrix} Y_I \\ Z_I+G \\ M_I \\ N_I \end{Bmatrix}; \tag{29}$$

$$\begin{Bmatrix} A \\ B \\ C \\ E \\ F \end{Bmatrix} = \begin{Bmatrix} \dfrac{\pi\rho D^3 C_{NA}}{8m} \\ \dfrac{\pi\rho p D^5 C_{YPA}(SL_{MAG}-SL_{CG})}{16I_y V_0} \\ \dfrac{\pi\rho D^4 C_{NA}(SL_{COP}-SL_{CG})}{8I_y} \\ \dfrac{\pi\rho D^5 C_{MQ}}{16I_y} \\ \dfrac{pDI_x}{I_y V_0} \end{Bmatrix}. \tag{30}$$

These equations are a coupled set of linear differential equations except for the fact that the total velocity, V, appears in the coefficients of many of the dynamic equations.

Projectile Linear Theory Solution

Liner theory offers physical insight into the flight dynamics since closed form solutions can be readily obtained [4]. Using the assumption that **V** changes slowly with respect to the other variables, it is thus considered to be constant, $\mathbf{V}\approx\mathbf{V}_0$, when it appears as a coefficient in all dynamic equations except its own. Moreover, pitch attitude of the projectile is regarded as constant in the velocity equation, uncoupling the velocity equation from the system. The angle of attack dynamics or epicyclic motion in Eq. (29), together with the roll dynamics in Eq. (28) are uncoupled and form a linear system of differential equations. In projectile linear theory, the Magnus force in Eqs. (25) and (26) is typically regarded as small in comparison to the other aerodynamic forces and is shown only for completeness. In further manipulation of the equations, all Magnus forces will be dropped. Magnus moments will be retained however, due to the magnitude amplification resulting from the cross product between Magnus force and its respective moment arm.

The solution to the differential equation (27), for the forward velocity, is

$$V(s) = \sqrt{V_0^2 e^{-2a_V s} + \frac{b_v}{a_v}(e^{-2a_v s}-1)}; \tag{31}$$

where

$$a_V = \frac{\rho S D C_{X0}}{2m}; \tag{32}$$

$$b_V = gD\theta_0. \tag{33}$$

When $\theta_0=0$, the velocity solution reduces to the familiar exponential decay form [4].

The roll dynamic equation is a nonhomogeneous linear differential equation with the following solution:

$$p(s)=\left(p_0+\frac{a_p}{b_p}V_0\right)e^{b_p s}-\frac{a_p}{b_p}V_0; \tag{34}$$

where

$$a_p=\frac{\rho SD^2C_{LDD}}{2I_{XX}}; \tag{35}$$

$$b_p=\frac{\rho SD^3C_{LP}}{4I_{XX}}. \tag{36}$$

In order to develop the swerve closed form solution, the epicyclic equations must first be solved because the lateral translation and rotational velocity components are contained in the attitude differential equations, and the attitudes are contained within the swerve differential equations. The epicyclic differential equations consist of a set of four coupled nonhomogeneous differential equations. The homogeneous solution is easily formed using the free vibration modes and mode shapes, and the results are given by the intrinsic complex expression

$$2\begin{Bmatrix} s_f \\ ss \\ \underline{s_f} \\ s_s \end{Bmatrix}=\begin{Bmatrix} (E-A)+iF\pm\sqrt{(E+A)^2-F^2+4C+2i((E+A)F+2B)} \\ (E-A)-iF\pm\sqrt{(E+A)^2-F^2+4C-2i((E+A)F+2B)} \end{Bmatrix}. \tag{37}$$

Calculating the sum and product of s_f and s_s leads the relations found in the next expression

$$\begin{Bmatrix} E-A \\ F \\ AE+C \\ -(AF+B) \end{Bmatrix}=\begin{Bmatrix} \lambda_f+\lambda_s \\ \Phi_f+\Phi_s \\ \Phi_f\Phi_s-\lambda_f\lambda_s \\ -(\lambda_f\Phi_s+\lambda_s\Phi_f) \end{Bmatrix}. \tag{38}$$

Two more simplifications based on size are introduced. First, neglect the product of damping and secondly, the product AE is neglected since the density ration is assumed small. A solution may now be obtained for both the fast and the slow damping factors and turning rates for the translational and rotational velocities.

$$\lambda_f=\frac{-(A-E)}{2}\left[1+\frac{F}{\sqrt{F^2-4C}}\left(1-\frac{(2AF+2B)}{F(A-E)}\right)\right]; \tag{39}$$

$$\Phi_f=\frac{1}{2}\left[F+\sqrt{F^2-4C}\right]; \tag{40}$$

$$\lambda_s=\frac{-(A-E)}{2}\left[1-\frac{F}{\sqrt{F^2-4C}}\left(1-\frac{(2AF+2B)}{F(A-E)}\right)\right]; \tag{41}$$

$$\Phi_s=\tfrac{1}{2}[F-\sqrt{F^2-4C}]. \tag{42}$$

Pulse Force and Moment Conditions

The pulse force applied to the projectile is taken to be a lateral impulsive force and this force is due to an actuator attached to the projectile body. [See the source terms of Eq. (29).] For this investigation the force actuator is modeled as a scaled square wave pulse so that the resulting force and moment components in the nonrolling frame are

$$Y_I=\frac{F^*V_0(\mathrm{sgn}(s-s_n)-\mathrm{sgn}(s-s_n-L_n))\cos\left(\frac{Dp}{V_0}s+\phi_B\right)}{2L_n}; \tag{43}$$

$$Z_I=\frac{F^*V_0(\mathrm{sgn}(s-s_n)-\mathrm{sgn}(s-s_n-L_n))\sin\left(\frac{Dp}{V_0}s+\phi_B\right)}{2L_n}; \tag{44}$$

$$M_I=-\frac{M^*V_0(\mathrm{sgn}(s-s_n)-\mathrm{sgn}(s-s_n-L_n))\sin\left(\frac{Dp}{V_0}s+\phi_B\right)}{2DL_n}; \tag{45}$$

$$N_I=\frac{M^*V_0(\mathrm{sgn}(s-s_n)-\mathrm{sgn}(s-s_n-L_n))\cos\left(\frac{Dp}{V_0}s+\phi_B\right)}{2DL_n}; \tag{46}$$

for a square wave pulse of length L_n that is initiated at s_n represented as

$$F^*=\frac{DF_d}{L_nmV_0^2}; \tag{47}$$

and

$$M^*=\frac{DF_dX_r}{L_nI_yV_0^2}. \tag{48}$$

Note the last two expressions become equivalent to delta function impulses in the limit of $L_n\to 0$.

Once the simplified mode shapes of Eq. (29) are obtained, the initial conditions for $\tilde{v}$, $\tilde{w}$, $\tilde{q}$, and $\tilde{r}$ are used to complete the solution. Equations (49) and (50) are the analytical solutions for the fixed plane translation velocities $\tilde{v}$ and $\tilde{w}$, expressed in phase-amplitude form,

$$\begin{aligned}\tilde{v}(s)=&V_1e^{\lambda_f s}\cos(\Phi_F s-\Theta_{V1})+V_2e^{\lambda_s s}\sin(\Phi_s s-\Theta_{V2})\\&+F_1(\Phi_f s,\Phi_s s)+F_2(\phi_B)\left(\frac{\mathrm{sgn}(s-s_n)-\mathrm{sgn}(s-s_n-L_n)}{2}\right)\\&+F_3(\phi_B)\left(\frac{\mathrm{sgn}(s-s_n-L_n)+1}{2}\right);\end{aligned} \tag{49}$$

$$\begin{aligned}\tilde{w}(s)=&V_1e^{\lambda_f s}\sin(\Phi_F s-\Theta_{V1})-V_2e^{\lambda_s s}\cos(\Phi_S s-\Theta_{V2})\\&+F_1\left(\Phi_f s-\frac{\pi}{2},\Phi_s s-\frac{\pi}{2}\right)+F_2\left(\phi_B-\frac{\pi}{2}\right)\\&\times\left(\frac{\mathrm{sgn}(s-s_n)-\mathrm{sgn}(s-s_n-L_n)}{2}\right)+F_3\left(\phi_B-\frac{\pi}{2}\right)\\&\times\left(\frac{\mathrm{sgn}(s-s_n-L_n)+1}{2}\right);\end{aligned} \tag{50}$$

where,

$$V_1=\sqrt{\left(\frac{(F-\Phi_f)\Phi_f\tilde{v}_0+\Phi_f(\tilde{w}_0E-\tilde{q}_0D)}{\Phi_f(\Phi_s-\Phi_f)}\right)^2+\left(\frac{\Phi_f(\tilde{w}_0(F-\Phi_f)-\tilde{v}_0E-\tilde{r}_0D)}{\Phi_f(\Phi_s-\Phi_f)}\right)^2}; \tag{51}$$

$$V_2=\sqrt{\left(\frac{(F-\Phi_s)\Phi_s\tilde{v}_0+\Phi_s(\tilde{w}_0E-\tilde{q}_0D)}{\Phi_s(\Phi_s-\Phi_s)}\right)^2+\left(\frac{\Phi_s(\tilde{w}_0(F-\Phi_s)-\tilde{v}_0E-\tilde{r}_0D)}{\Phi_s(\Phi_s-\Phi_f)}\right)^2}; \tag{52}$$

$$\Theta_{V1}=\tan^{-1}\left(\frac{\Phi_f(\tilde{w}_0(F-\Phi_f)-\tilde{v}_0E-\tilde{r}_0D)}{(F-\Phi_f)\Phi_f\tilde{v}_0+\Phi_f(\tilde{w}_0E-\tilde{q}_0D)}\right); \tag{53}$$

$$\Theta_{V2}=\tan^{-1}\left(\frac{(F-\Phi_s)\Phi_s\tilde{v}_0+\Phi_s(\tilde{w}_0E-\tilde{q}_0D)}{\Phi_s(\tilde{w}_0(F-\Phi_s)-\tilde{v}_0E-\tilde{r}_0D)}\right); \tag{54}$$

$$F_1(\Phi_f s,\Phi_s s)=\frac{Ge^{\lambda_f s}[((P-\Phi_f)F-P\Phi_f+\Phi_f^2)\cos(\Phi_f s)+(P-\Phi_f)E\sin(\Phi_f s)]}{\Phi_f(P-\Phi_f)(\Phi_s-\Phi_f)}$$
$$-\frac{Ge^{\lambda_s s}[((\Phi_s-P)F-\Phi_s^2+P\Phi_s)\cos(\Phi_s s)+(\Phi_s-P)E\sin(\Phi_s s)]}{\Phi_s(\Phi_s-P)(\Phi_s-\Phi_f)}-\frac{FG}{\Phi_f\Phi_s}; \tag{55}$$

$$F_2(\phi_B)=\frac{V_0e^{\lambda_f(s-s_n)}[(\Phi_f-F)F^*\sin\Omega_f+(M^*+EF^*)\cos\Omega_f]}{(\Phi_s-\Phi_f)(P-\Phi_f)L_n}-\frac{V_0e^{\lambda_s(s-s_n)}[(\Phi_f-F)F^*\sin\Omega_s+(M^*+EF^*)\cos\Omega_s]}{(\Phi_s-\Phi_f)(P-\Phi_s)L_n}$$
$$+\frac{V_0[F^*(P-F)\sin(Ps+\phi_B)+(M^*+EF^*)\cos(Ps+\phi_B)]}{(P-\Phi_f)(P-\Phi_s)L_n}; \tag{56}$$

$$F_3(\phi_B)=\frac{V_0e^{\lambda_f(s-L_n-s_n)}\{e^{\lambda_fL_n}((M^*+EF^*)\cos\Omega_f+(\Phi_f-F)F^*\sin\Omega_f)-(F-\Phi_f)F^*\sin\Delta_f-(M^*+EF^*)\cos\Delta_f\}}{(\Phi_s-\Phi_f)(P-\Phi_f)L_n}$$
$$-\frac{V_0e^{\lambda_s(s-L_n-s_n)}\{e^{\lambda_sL_n}((M^*+EF^*)\cos\Omega_s+(F-\Phi_s)F^*\sin\Omega_s)-(F-\Phi_f)F^*\sin\Delta_f-(M^*+EF^*)\cos\Delta_f\}}{(\Phi_s-\Phi_f)(P-\Phi_s)L_n}; \tag{57}$$

$$P=\frac{Dp}{V_0}; \tag{58}$$

$$\Omega_f=(P-\Phi_f)s_n+\phi_B+\Phi_f s,\quad \Omega_s=-(P-\Phi_s)s_n-\phi_B-\Phi_s s; \tag{59}$$

$$\Delta_f=(P-\Phi_f)L_n+\Omega_f,\quad \Delta_s=(P-\Phi_f)L_n-\Omega_s. \tag{60}$$

Swerving motion is measured along the earth-fixed $\mathbf{J_I}$ and $\mathbf{K_I}$ axes. To an observer standing behind the gun tube, these axes are oriented such that positive $\mathbf{J_I}$ is to the right and positive $\mathbf{K_I}$ is pointed downward. The swerving motion results from a combination of the normal aerodynamic forces, as the projectile pitches and yaws, plus the forces and moments due to the applied impulse. Differentiating Eqs. (22) and (23) with respect to nondimensional arc length, generates the swerve equations such that

$$\left(\frac{y}{D}\right)''=\frac{F^*(\mathrm{sgn}(s-s_n)-\mathrm{sgn}(s-s_n-L_n))\cos(ps+\phi_B)}{2L_n}-\frac{A\tilde{v}}{V_0}; \tag{61}$$

$$\left(\frac{z}{D}\right)''=\frac{F^*(\mathrm{sgn}(s-s_n)-\mathrm{sgn}(s-s_n-L_n))\sin(ps+\phi_B)}{2L_n}$$
$$+\frac{G-A\tilde{w}}{V_0}; \tag{62}$$

Integrating these equations is straightforward but the solutions are judged to be too long to be listed here. However, the asymptotic limit of these solutions, $s\to\infty$, is of special interest.

For a stable projectile, the swerve caused by epicyclical vibration decays as the projectile progresses downrange and does not affect the long-term lateral motion of the projectile. When a lateral pulse is applied to the projectile at arc length s_n, its effect on the target impact point is predominantly due to induced jump, provided the target distance is sufficient to allow the transients to decay. Projectile linear theory shows that the long-term center of mass solution, or swerve, contains terms that remain bounded with arc length s plus terms that are linear with s and if gravity is included the solution will have even higher order diverging terms. These higher order terms are typically denoted as gravity drop. The linear terms are called jump terms, which are caused by initial conditions at the gun muzzle, lateral pulse forces, and aerodynamic characteristics. Mathematically, setting gravity to zero and subsequently evaluating the following limits formally defines aerodynamic jump

$$\lim_{s\to\infty}\frac{y(s)}{Ds}=\Gamma_J\quad \lim_{s\to\infty}\frac{z(s)}{Ds}=\Gamma_K. \tag{63}$$

The total aerodynamic jump vector Γ is expressed as the sum of two vectors. The first vector represents the muzzle conditions and the second results from the lateral pulse force and moment:

$$\begin{Bmatrix}\Gamma_J\\ \Gamma_K\end{Bmatrix}=-\frac{A}{[(AF+B)^2+(AE+C)^2]V_0}\begin{Bmatrix}AF+B & -AE-C\\ AE+C & AF+B\end{Bmatrix}$$
$$\times\begin{Bmatrix}v_0F+w_0E-q_0D\\ w_0F-v_0E-r_0D\end{Bmatrix}+\Lambda\begin{Bmatrix}\cos\Pi\\ \sin\Pi\end{Bmatrix}; \tag{64}$$

for which

$$Y=\frac{A(AF+B)M^*+A(BE-CF)F^*}{(AF+B)^2+(AE+C)^2}$$
$$Z=\frac{(ABF+ACE+C^2+B^2)F^*-A(AE+C)M^*}{(AF+B)^2+(AE+C)^2}$$
$$\Pi=\tan^{-1}(Z/Y)-\frac{PL_n}{2}-Ps_n-\phi_B\to\tan^{-1}(Z/Y)-Ps_n-\phi_B\ \text{ as }\ L_n\to0$$
$$\Lambda=\sqrt{Y^2+Z^2}\frac{\sin(PL_n/2)}{(PL_n/2)}\to\sqrt{Y^2+Z^2}\ \text{ as }\ L_n\to0. \tag{65}$$

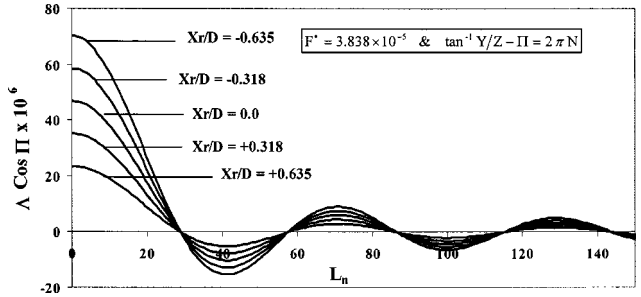

Fig. 3 (*A*) Surface speckle pattern; (*B*) Shifted surface speckle pattern

The quantities Λ and Π are the magnitude and phase angle of the jump vector attributed to the lateral pulse. It is interesting to note that the jump terms induces by the lateral pulse are not dependent on the lateral state of the projectile ($\tilde{v}(s)$, $\tilde{w}(s)$, $\tilde{q}(s)$, and $\tilde{r}(s)$), thus this particular contribution to jump is not coupled to the projectile's angle of attack. Equation (65) extends the work by Guidos and Cooper [6] who considered nonspinning projectiles subject to a singular, delta function, impulse. Limiting $(L_n, P) \rightarrow 0$ in Eqs. (64) and (65) produces expressions that agree with their previous predictions.

Lateral Pulse Smearing

In order to better understand the swerve response due to a lateral pulse, results for a representative spin-stabilized 40-mm projectile configuration are calculated and discussed in this and the next two sections. Nominal values for the aerodynamic coefficients, the projectile physical parameters, and flight characteristics are given in the Appendix. All results presented use these values unless specified differently. Diversions from these nominal values are clear from the context of the particular chart under examination.

Plots showing the effect of smearing are given in Fig. 3 and Fig. 4 for the applied force $F^* = 3.838 \times 10^{-5}$ and moments arms $X_r/D = [-0.635 \xrightarrow{\text{to}} +0.635]$. Negative values of X_r indicate the application point of the pulse force is aft of the mass center while positive values indicate the pulse force is forward of the mass center. To illustrate the smearing effects the roll position, ϕ_N, of the lateral impulse force is assumed to act primarily along the nonrolling Y-axis. This means the arc length, s_N, corresponding to the center of the pulse satisfies the expression $\phi_N = \phi' s_N + \phi_B = 2\pi N$, $N = 0,1,2,\ldots$. To assure this force is acting nominally along the no rolling Y-axis the activation point begins at $s_n = s_N - L_n/2$ so that the duration of the impulse brackets $\phi_N = 2\pi N$. Increasing pulse length, L_n, causes the jump components to cyclically decay while its value at $L_n = 0$ corresponds to a lateral impulse that is proportional to the delta function $\delta(s - s_n)$. Values of L_n where the jump is zero represent situations where the duration of the lateral pulse coincides with a roll cycle. This accounts for the post multiplier, $\sin(pDL_n/2V_0)$, in Eq. (65) having 2π zero crossings and causes the cyclical jump results in Fig. 3 and Fig. 4. Notice for the cases presented, the response due to a

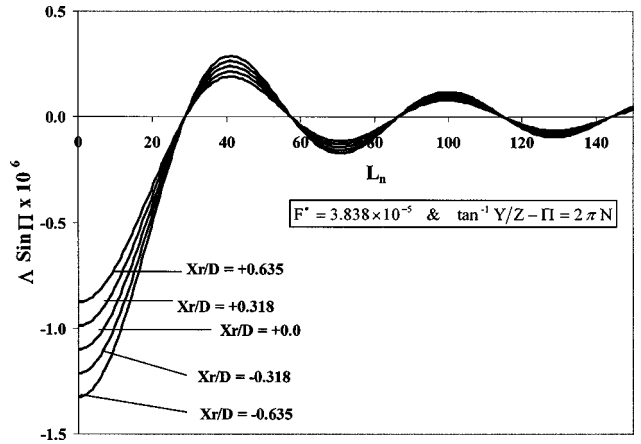

Fig. 4 Local deformation

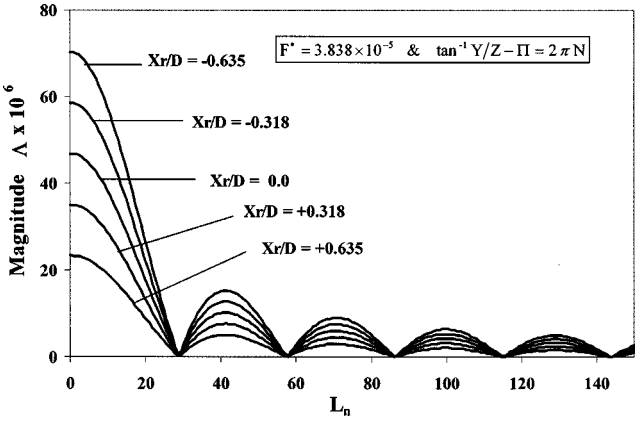

Fig. 5 Cost surface

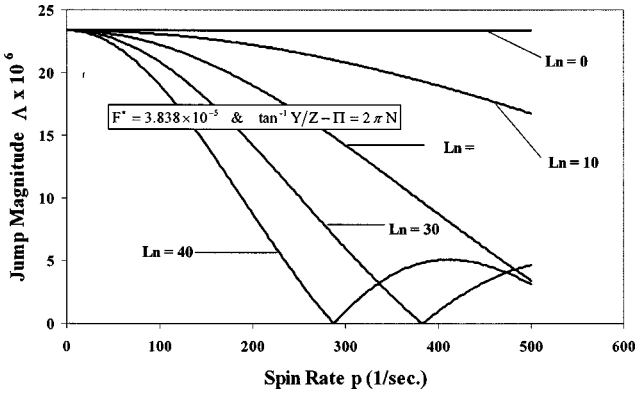

Fig. 6 Crossover and blending of parent chromosomes

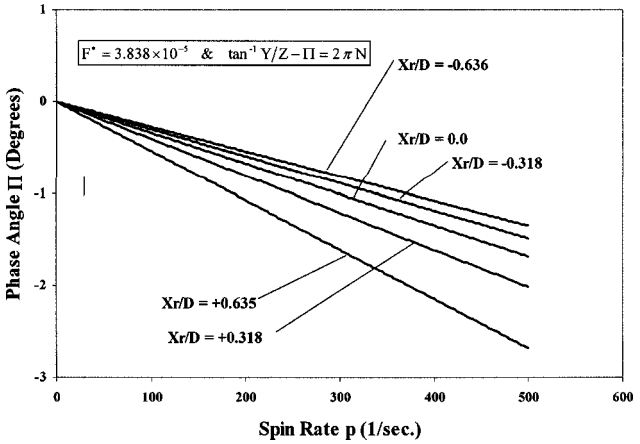

Fig. 7 A single series of results for the calibration routine

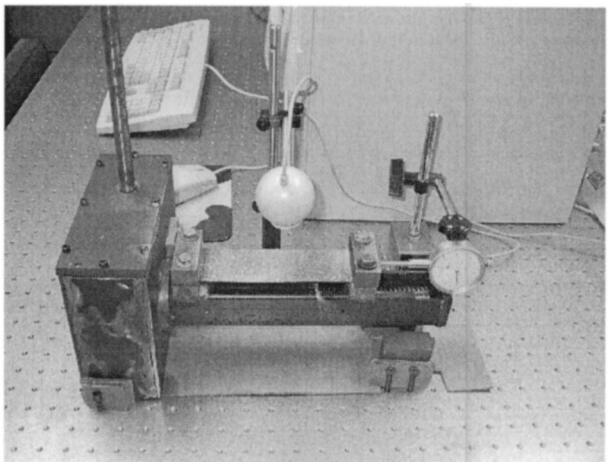

Fig. 8 Experimental setup

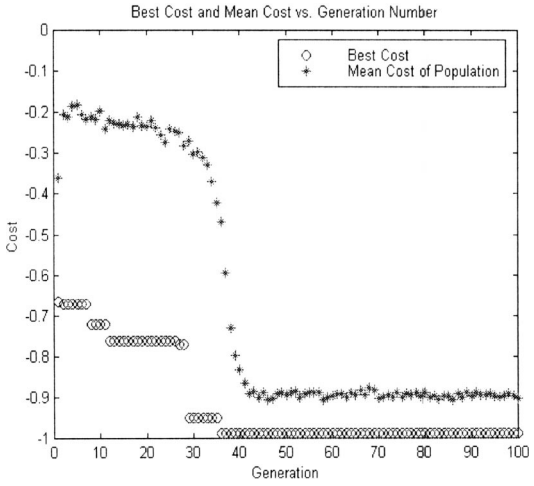

Fig. 9 Best cost and mean vs generation

pulse in the $\mathbf{J_I}$ direction is predominantly along $\mathbf{J_I}$ however, a smaller out of phase component of swerve is also generated.

Lateral Pulse Response Magnitude and Phase Angle

Figure 5 has charts showing the absolute value of Λ as a function of the pulse length L_n for the previous parameter values $F^* = 3.838 \times 10^{-5}$ and $X_r/D = [-0.635 \xrightarrow{\text{to}} +0.635]$. Here again the impulse is assumed to bracket $\phi_N = 2\pi N$. The maximum value occurs at $L_n = 0$, which is the delta function result, as is justified from Eq. (65). Consideration of Λ as a function of spin rate p is displayed in Fig. 6 for several pulse durations, $L_n = [0 \xrightarrow{\text{to}} 40]$. This figure shows that the rate at which the aerodynamic jump magnitude decreases, with spin rate, is strongly dependent on the pulse duration. Again, this is attributed to smearing effects, which become more pronounced with increasing values of L_n.

Figure 7 gives the phase angle, Π, [see Eq. (65)] as a function of spin rate for the same values of the moment arm length X_r/D discussed above. Notice that the phase angle linearly increases with spin rate, indicating that spin stabilized projectiles are most susceptible to an out of phase swerve response due to lateral pulse forces.

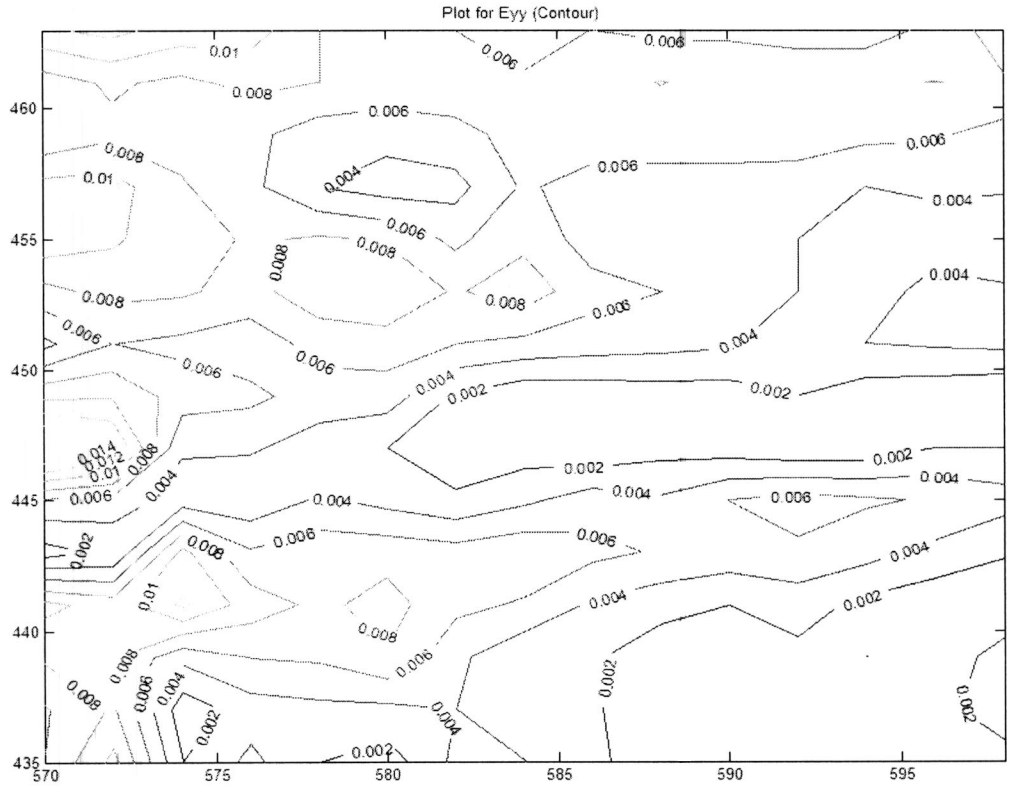

Fig. 10 2D strain contours next to a hole in plate loaded vertically

Target Interception

The last topic discussed in this paper examines the relationship between a given change in aerodynamic jump, $\{^{\Delta\Gamma_J}_{\Delta\Gamma_K}\}$, and the impulse needed to create this change. This may be desirable when the activated impulse is strong enough to force a projectile to strike its target, located at a relative position $\{^{\Delta\Gamma_J}_{\Delta\Gamma_K}\}$, with a single impulse. Hence Eq. (64) requires

$$\begin{Bmatrix} \Delta\Gamma_J \\ \Delta\Gamma_K \end{Bmatrix} = \Lambda \begin{Bmatrix} \sin\Pi \\ \cos\Pi \end{Bmatrix}. \tag{66}$$

Solving this system for Π while insisting that Π remain real valued yields the following two equations for target interception.

$$\sin^2\left(\frac{pDs_n}{2V_0}\right) = \frac{pDs_n(\Delta\Gamma_J+\Delta\Gamma_K)}{2V_0(\Sigma_J^2+\Sigma_K^2)}; \tag{67}$$

$$\frac{pDs_n}{V_0} + \phi_B = -\frac{pDL_n}{2V_0} + \tan^{-1}\left(\frac{\Delta\Gamma_K\Sigma_J - \Delta\Gamma_J\Sigma_K}{\Delta\Gamma_J\Sigma_J + \Delta\Gamma_K\Sigma_K}\right) + 2\pi N. \tag{68}$$

Using Eq. (65) the impulse force F_I can be determined from Eq. (67), for a given moment arm X_r, and then Eq. (68) solved for ϕ_B will guarantee target impact provided the relative target position, $\{^{\Delta\Gamma_J}_{\Delta\Gamma_K}\}$, is known (see Figs. 8–10).

Conclusions

An analytical approach for quantifying the effect of a lateral square impulse disturbing a projectile during free flight has been presented. All of the analysis was based on projectile linear theory, which produces simple closed form solutions for the assumed square pulse disturbance. These solutions are then used to calculate the projectile swerving motion, so that the long-term effects of the lateral impulse are readily determined. The primary interest regarding target interception is the projectile's aerodynamic jump. Changes to aerodynamic jump caused by the lateral impulse forces was shown to produce easy to understand additive contributions to the usual aerodynamic jump of a free flight projectile with no applied impulse.

The important question concerning smearing effects originating from a finite length pulse has been addressed where pulse induced control authority is shown to diminish as $1/L_n$. Calculations also show the additional aerodynamic jump magnitude, Σ, decreases with spin rate p when subjected to various pulse lengths L_n.

Nomenclature

C_i = Projectile aerodynamic coefficients
D = Projectile characteristic length (diameter)
F_d = Dimensional impulse force
g = Gravitational constant
G = Scaled gravitational constant $G = gD/V_0$
I_X, I_Y = Mass moments of inertia
$\tilde{L}$, $\tilde{M}$, $\tilde{N}$ = Applied moments about projectile mass center expressed in the no-roll frame
m = Projectile mass
p, $\tilde{q}$, $\tilde{r}$ = Angular velocity components vector of projectile in the no-roll frame
S = Surface area $S = \pi D^2/4$
s = Nondimensional arch length
$\mathrm{sgn}(\tau)$ = $\{^{\tau/|\tau|\ \tau\neq 0}_{0\ \tau=0}$
u, v, w = Mass center velocity components in the body reference frame
V_0 = Forward velocity of projectile
u, $\tilde{v}$, $\tilde{w}$ = Mass center velocity components in the no-roll reference frame
X_r = Dimensional moment arm length
Y_I, Z_I = Applied force components in the no-roll reference frame
$\begin{Bmatrix} x \\ y \\ z \end{Bmatrix}$ = Position vector of body center of mass in an inertial reference frame
α = Longitudinal aerodynamic angle of attack
β = Lateral aerodynamic angle of attack
Λ_K, Λ_J = ^J_K Components of aerodynamic jump due to lateral impulse
Π = Phase angle of the aerodynamic jump due to lateral impulse
ϕ, θ, ψ = Euler roll, pitch, and yaw angles of the projectile
ϕ_B = Euler roll angle of the applied impulse

Appendix

The numerical values used for the graphical presentations given in this report are shown in the following matrices:

$$\text{Aerodynamic coefficients} \mapsto \begin{Bmatrix} C_{X0} \\ C_{X2} \\ C_{NA} \\ C_{YPA} \\ C_{LP} \\ C_{MQ} \end{Bmatrix} = \begin{Bmatrix} 0.279 \\ 2.672 \\ 2.329 \\ -0.295 \\ -0.042 \\ -1.800 \end{Bmatrix}$$

$$\text{Physical parameters} \mapsto \begin{Bmatrix} m \\ I_X \\ I_Y \\ D \\ SL_{COP} \\ SL_{MAG} \\ SL_{CG} \end{Bmatrix} = \begin{Bmatrix} 0.0116\ \ Slug \\ 2.85\times10^{-5}\ \ \text{Slug ft.}^2 \\ 2.72\times10^{-5}\ \ \text{Slug ft.}^2 \\ 0.137\ \ \text{ft.} \\ 0.237\ \ \text{ft.} \\ 0.239\ \ \text{ft.} \\ 0.0713\ \ \text{ft.} \end{Bmatrix}$$

$$\text{Flight characteristics} \mapsto \begin{Bmatrix} \rho \\ V_0 \\ p \end{Bmatrix} = \begin{Bmatrix} 2.38\times10^{-3}\ \ \text{Slug ft.}^{-3} \\ 250.0\ \ \text{ft. s}^{-1} \\ 399.7\ \ \text{s}^{-1} \end{Bmatrix}.$$

References

[1] Harkins, T. E., and Brown, T. G., 1999, "Using Active Damping as a Precision-Enhancing Technology for 2.75-Inch Rockets," U.S. Army Research Laboratory, Aberdeen Proving Ground, MD, ARL-TR-1772.
[2] Jitpraphai, T., and Costello, M., 2001, "Dispersion Reduction of a Direct Fire Rocket Using Lateral Pulse Jets," J. Spacecr. Rockets, **38**, pp. 929–936.
[3] Amitay, M., Smith, D., Kibens, V., Parekh, D., and Glezer, A., 2001, "Aero-

dynamic Flow Control Over an Unconventional Airfoil Using Synthetic Jet Actuators,'' AIAA J., **39**, pp. 361–370.
[4] Murphy, C. H., 1963, ''Free Flight Motion of Symmetric Missiles,'' BRL Report No. 1216, U.S. Army Ballistic Research Laboratories, Aberdeen Proving Ground, MD.
[5] McCoy, R. L., 1999, Modern Exterior Ballistics: The Launch and Flight Dynamics of Symmetric Projectiles, Schiffer Publishing Ltd., Atglen, PA.
[6] Guidos, B., and Cooper, G., 2002, ''Linearized Motion of a Fin-Stabilized Projectile Subjected to a Lateral Impulse,'' J. Spacecr. Rockets, **39**, pp. 384–39.